Published OnlineFirst October 21, 2011; DOI:10.1158/1078-0432.CCR-11-0608

Clinical Cancer Research

Imaging, Diagnosis, Prognosis

In Vivo Positron Emission Tomography Imaging of Protease Activity by Generation of a Hydrophobic Product from a Noninhibitory Protease Substrate

Chih-Hung Chuang[1], Kuo-Hsiang Chuang[3], Hsin-Ell Wang[9], Steve R. Roffler[10], Jen-taie Shiea[6,7], Shey-Cherng Tzou[3], Ta-Chun Cheng[5], Chien-Han Kao[5], Shih-Yen Wu[9], Wei-Lung Tseng[6,7], Chiu-Min Cheng[8], Ming-Feng Hou[4], Ju-Ming Wang[1,2], and Tian-Lu Cheng[3,4,5]

Abstract

Purpose: To develop an imaging technology for protease activities in patients that could help in prognosis prediction and in design of personalized, protease-based inhibitors and prodrugs for targeted therapy.

Experimental Design: Polyethylene glycol (PEG) was covalently attached to the N-terminus of a hydrophilic peptide substrate (GPLGVR) for matrix metalloproteinase (MMP) to increase hydrophilicity. PEG-peptide was then linked to a hydrophobic tetramethylrhodamine (TMR) domain and labeled with ^{18}F to form a PEG-peptide-^{18}F-TMR probe. Specific cleavage of the probe by MMP2 was tested *in vitro* by matrix-assisted laser desorption/ionization–time-of-flight (MALDI-TOF). *In vivo* imaging of MMP2-expressing tumors was evaluated by micro-PET.

Results: The hydrophobic TMR fragment (948 Da) was specifically generated by MMP2 enzymes and MMP-expressing HT1080 cells but not control MCF-7 cells. MMP-expressing HT1080 cells and tumors selectively accumulated the hydrolyzed, hydrophobic TMR fragment at sites of protease activity. Importantly, we found that ^{18}F-labeled probe (^{18}F-TMR) preferentially localized in HT1080 tumors but not control MCF-7 tumors as shown by micro-PET. Uptake of the probe in HT1080 tumors was 18.4 $\pm$ 1.9-fold greater than in the MCF-7 tumors 30 minutes after injection. These results suggest that the PEG-peptide-^{18}F-TMR probe displays high selectivity for imaging MMP activity.

Conclusions: This strategy successfully images MMP expression *in vivo* and may be extended to other proteases to predict patient prognosis and to design personalized, protease-based inhibitors and prodrug-targeted therapies. *Clin Cancer Res; 18(1); 238–47. ©2011 AACR.*

Authors' Affiliations: [1]Institute of Basic Medical Sciences, [2]Institute of Bioinformatics and Biosignal Transduction, National Cheng Kung University, Tainan; Departments of [3]Biomedical Science and Environmental Biology and [4]Surgery, Cancer Center, [5]Graduate Institute of Medicine, Kaohsiung Medical University Hospital; [6]Department of Chemistry, National Sun Yat-Sen University; [7]National Sun Yat-Sen University-Kaohsiung Medical University Joint Research Center; [8]Department of Aquaculture, National Kaohsiung Marine University, Kaohsiung; [9]Faculty of Biomedical Imaging and Radiological Sciences, National Yang-Ming University; and [10]Institute of Biomedical Sciences, Academia Sinica, Taipei, Taiwan

Note: Supplementary data for this article are available at Clinical Cancer Research Online (http://clincancerres.aacrjournals.org/).

C.-H. Chuang and K.-H. Chuang contributed equally to the study.

Corresponding Author: Tian-Lu Cheng, Department of Biomedical and Environmental Biology, Kaohsiung Medical University, 100 Shih-Chuan 1st Road, Kaohsiung, Taiwan. Phone: 886-7-3121101-2697; Fax: 886-7-3227508; E-mail: tlcheng@kmu.edu.tw and Ju-Ming Wang, Institute of Bioinformatics and Biosignal Transduction, National Chen Kung University, 1 University Road, Tainan 701, Taiwan. Phone: 886-6-2757575-31067; Fax: 886-6-2083663; E-mail: yumingw@mail.ncku.edu.tw

doi: 10.1158/1078-0432.CCR-11-0608

Introduction

Proteases are involved in tumor formation, angiogenesis, local invasion, and metastatic spread (1–3). Members of the matrix metalloproteinase (MMP) family contribute to the invasion and metastasis of bladder cancer, fibrosarcoma, breast cancer, and colon cancer (4, 5). Given their relevance in cancer biology, proteases are attractive targets for the design of anticancer drugs that act preferentially at cancer sites. In line with this notion, several protease inhibitors, such as the MMP inhibitors marimastat (6), AG3340 (7), S-3304 (8), and BAY 12-9566 (9), have entered phase I, II, and III clinical trials for cancer therapy. In addition, many protease substrate prodrugs have been reported to inhibit the growth of several cancer types *in vivo* (10, 11). On the other hand, many studies have also shown a clear correlation between protease expression and poor prognosis of patients with cancer (12–14), indicating that proteases may be useful as markers to predict tumor recurrence and

Published OnlineFirst October 21, 2011; DOI:10.1158/1078-0432.CCR-11-0608

Translational Relevance

Development of a noninhibitory imaging strategy for visualizing *in vivo* protease activity would aid in determining patient prognosis and designing personalized, protease-based inhibitors and prodrugs for targeted therapy. Here, we developed an imaging strategy based on the conversion of a noninhibitory protease substrate probe (PEG-peptide-^{18}F-TMR) to a hydrophobic probe (^{18}F-TMR) that allows *in vitro* and *in vivo* detection of protease activity by micro–positron emission tomography (PET). Our results show that PEG-peptide-TMR was specifically hydrolyzed to TMR and accumulated at MMP-expressing HT1080 cells *in vitro* and *in vivo*. By using PET imaging, we found that ^{18}F-TMR preferentially accumulated in MMP-expressing HT1080 tumors but not in control MCF-7 tumors. Conceptually, the protease substrate in our probe could be replaced to detect other protease-associated diseases. Therefore, this new noninhibitory protease probe may have broad utility for clinical and experimental medicine.

prognostic survival. Thus, tumor-associated proteases seem attractive as both therapeutic targets and prognosis markers. Therefore, the technology to image protease activity *in vivo* would provide a valuable tool to design personalized, protease activity–based prodrug therapies and to monitor tumor recurrence and patient prognosis.

However, imaging systems are not yet available for clinical imaging of protease activities. Optical imaging is thus far the most widely used approach to detect protease activity *in vivo*. For example, protease-activatible near infrared fluorescence (NIRF) imaging probes have been used to image MMPs (15), uPA (16), and cathepsin B (17) activity in small animals. However, the shallow penetration of the excitation/emission spectrum still limits clinical use in human. Recently, a protease-activated solubility-convertible contrast agent (Gd-DOTA-MMP2 peptide) was developed for the imaging of MMP activity by MRI (18). However, low spatial sensitivity of MRI and the relatively large quantity of probe required may hinder its clinical applications. On the other hand, protease inhibitors labeled with radioisotopes have been developed for single-photon emission computed tomography (SPECT) or positron emission tomography (PET) imaging. Radiolabeled protease inhibitors could bind to the catalytic site of MMP2/9 (19, 20) and MMP14 (21) for *in vivo* imaging. However, inhibitor-based imaging agents may bind indiscriminately to both the active and latent form of proteases which may lead to inaccurate interpretation of protease activities. Furthermore, these inhibitor-based imaging agents may inhibit protease activity *in vivo*, excluding the concurrent application for protease-based prodrugs targeted therapy. Therefore, development of a noninhibitory yet highly sensitive and specific activity–based PET imaging probe is desirable to improve cancer patient management.

To overcome these challenges, we linked a hydrophilic polyethylene glycol (PEG_{5000}) molecule to the N-terminus of a MMP2/9 peptide substrate (GPLGVR; ref. 22), then attached PEG-peptide to a hydrophobic tetramethylrhodamine group (TMR), and finally labeled ^{18}F to form a PEG-peptide-^{18}F-TMR probe (Fig. 1). Upon protease cleavage, the hydrophobic ^{18}F-TMR is released and preferentially accumulates at sites displaying protease activity. The radioactivity from ^{18}F-TMR is then detected by PET to diagnose protease activity *in vivo* (Fig. 1). In this report, we first used matrix-assisted laser desorption/ionization–time-of-flight (MALDI-TOF) to examine hydrolysis of peptide-TMR by purified MMP2 and MMP-expressing HT1080 cells. We then examined whether hydrophobic TMR could be selectively retained at MMP-expressing HT1080 cells/tumors but not in control MCF-7 cells/tumors *in vitro* and *in vivo*. Finally, we evaluated whether MMP-positive tumors could hydrolyze PEG-peptide-^{18}F-TMR and accumulate ^{18}F-TMR for detection by micro-PET imaging in mice. We report that MMP-expressing tumors can be imaged by this strategy, which may help to develop personalized, protease-based targeted therapies and to evaluate cancer prognosis based on the protease profile in the patients.

Materials and Methods

Cells and animals

The human fibrosarcoma cell line HT1080 and the human breast adenocarcinoma cell line MCF-7 were purchased from the American Type Culture Collection. The cells were cultured in Dulbecco's Modified Eagle's Medium (DMEM; Sigma-Aldrich) supplemented with 10% heat-inactivated bovine calf serum, 100 units/mL penicillin, and 100 μg/mL streptomycin (Sigma-Aldrich) at 37°C in a humidified atmosphere of 5% CO_2. Female BALB/c nude mice (6–8 weeks old) were obtained from the National Laboratory Animal Center, Taipei, Taiwan. All animal experiments were carried out in accordance with institutional guidelines and approved by the Animal Care and Use Committee of the Kaohsiung Medical University, Kaohsiung, Taiwan.

Synthesis of peptide-TMR and PEG-peptide-TMR

Peptide-TMR (Cys-Arg-Ser-Gly-Pro-Leu-Gly-Val-Lys-Lys-TMR) was synthesized by Gu-Yuan Inc. and purified to more than 95% purity by high-performance liquid chromatography [HPLC; Merck Hibar C18 column, 4 × 250 mm; eluted at 1 mL/min with a gradient starting from 95% solvent A (0.1% trifluoroacetic acid in water) and 5% solvent B (0.1% trifluoroacetic acid in MeCN) to 5% solvent A and 95% solvent B at 30 minutes]. The mass spectrum of the peptide-TMR was confirmed by MALDI-TOF. The N-terminal cysteine of the peptide-TMR was reacted with methoxy PEG maleimide (mPEG-MAL; Sigma-Aldrich) at a molar ratio of 1:2 in PBS at room temperature for 4 hours to form PEG-peptide-TMR. The free PEG was removed by

Published OnlineFirst October 21, 2011; DOI:10.1158/1078-0432.CCR-11-0608

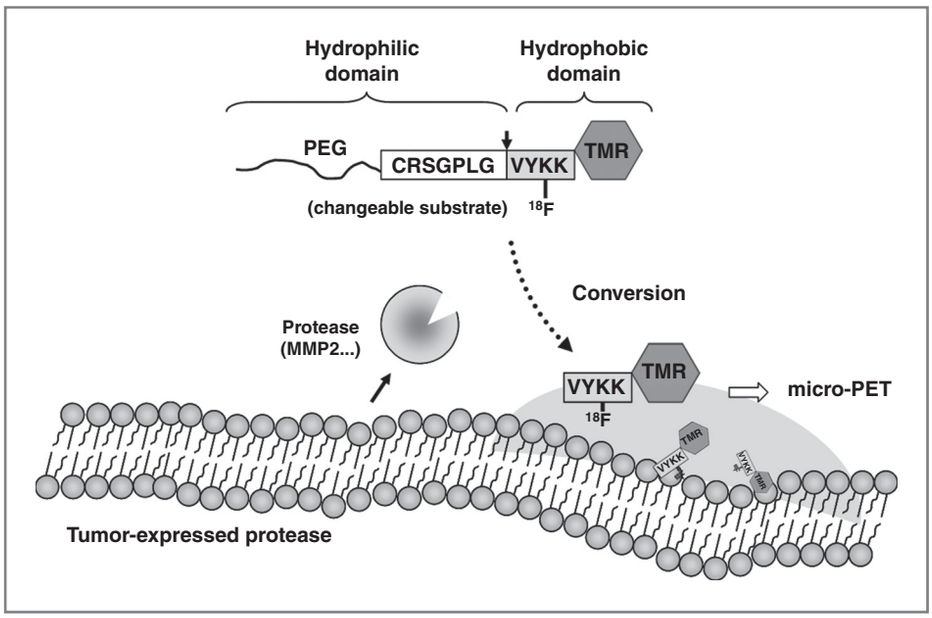

Figure 1. Schematic representation of the protease activity–based micro-PET strategy. The protease substrate probe (PEG-peptide-^{18}F-TMR) consists of a hydrophilic PEG (PEG_{5000}) molecule coupled to a ^{18}F-labeled peptide containing a MMP2/9 cleavage site (GPLGVR) and hydrophobic TMR moiety. Upon proteolytic cleavage, the hydrophobic ^{18}F-TMR moiety preferentially accumulates at sites displaying protease activity. The radiation from ^{18}F-TMR is then detected by PET to indicate the site of the protease activity *in vivo*.

Sephadex G25 column chromatography (Roche Applied Science), and the purity of the final compound was assessed by HPLC to be around 80% to 90%.

Analysis of the hydrolysis of peptide-TMR by MALDI-TOF

Peptide-TMR (10 μmol/L) was incubated with either 1 unit of purified MMP2 (AnaSpec) or the serum-free culture medium of HT1080 cells or MCF-7 cells at 37°C for 1 hour, respectively. Each sample was mixed 1:1 with the MALDI matrix, cyano-4-hydroxycinnamic acid (CHC; Sigma-Aldrich). The mixture was deposited on the MALDI sample plate. After drying, the sample was analyzed using a MALDI-TOF mass spectrometer (Autoflex; Bruker Daltonics) running the Flexcontrol 1.2 software package version 3. The sample spot was irradiated with a pulsed nitrogen laser (337 nm with a pulsed width of 4 ns) for desorption and ionization. For each sample spot, 500 laser shots were averaged to obtain representative mass spectra. All positive-ion mass spectra were acquired in the linear ion mode at an acceleration voltage of 20 kV under the delayed extraction mode.

In vitro activation of the PEG-peptide-TMR

A total of 1×10^5 HT1080 or MCF-7 cells were seeded with DMEM containing 10% serum in a 24-well plate at 37°C in a CO_2 incubator overnight. The cells were cultured in serum-free DMEM for 48 hours before addition of 2.5 or 5 μmol/L PEG-peptide-TMR in the presence or absence of 20 μg/mL purified MMP2 (AnaSpec) at 37°C for 1 hour. After washing with PBS, the fluorescence of viable cells was observed under a fluorescence microscope (Axiovert 200; Carl Zeiss MicroImaging). To investigate whether the fluorescence signal was inhibited by protease inhibitors, the cells were also stained with 5 μmol/L peptide-TMR in the presence or absence of 10 μmol/L 1,10-phenanthroline (Sigma-Aldrich; refs. 23, 24) at 37°C for 1 hour. After washing with PBS, the fluorescence of viable cells was measured with a flow cytometer (Becton Dickinson) and analyzed with FlowJo V3.2 (Tree Star, Inc.).

In vivo optical imaging of MMP activity

BALB/c nude mice ($n = 3$) bearing established HT1080 and MCF-7 tumors (100–200 mm^3) in their right and left hind legs, respectively, were anesthetized by halothane vapor with a vaporizer system and then were intravenously injected with 350 μmol/L (100 μL PBS) PEG-peptide-TMR. Optical images were sequentially obtained at 30, 60, and 90 minutes with a NightOWL II LB 983 NC100 image system (Berthold Technologies). The fluorescence intensities were analyzed with IndiGo Basic version 1.2 (Berthold Technologies) analysis software.

Histologic analysis of the fluorescence intensity and protease activity in tumors

BALB/c nude mice ($n = 3$) bearing established HT1080 and MCF-7 tumors (100–200 mm^3) in their right and left hind legs, respectively, were intravenously injected with 350 μmol/L (in 100 μL) PEG-peptide-TMR and sacrificed 1 hour later. Tumors were excised and embedded in optimum cutting temperature (OCT) compound (Tissue-Tek) in liquid nitrogen. Consecutive sections (10 μm) were stained for protease activity with a 520 MMP-2 Assay Kit (AnaSpec) according to the manufacturer's instructions. The sections were examined on an upright BX4 microscope (Olympus) or viewed under phase contrast or fluorescence fields on an inverted Axiovert 200 microscope (Carl Zeiss Microimaging). The results of MMP activity were then matched to the region of peptide-TMR accumulation.

Published OnlineFirst October 21, 2011; DOI:10.1158/1078-0432.CCR-11-0608

Synthesis and purification of PEG-peptide-^{18}F-TMR

N-succinimidyl 4-[^{18}F]fluorobenzoate (^{18}F-SFB) was synthesized from *tert*-butyl 4-*N*,*N*,*N*-trimethylammonium-benzoate triflate (Sigma-Aldrich) as previously reported with minor modifications (25). ^{18}F-SFB was obtained in the decay-corrected radiochemical yields of 40% to 50% and a radiochemical purity of more than 95%. The ^{18}F-SFB was dissolved in 50 μL of dimethyl sulfoxide and was incubated with PEG-peptide-TMR (0.6 mg) in 0.6 mL of phosphate buffer (0.1 N, pH 8.5) for 30 minutes at 55°C. PEG-peptide-^{18}F-TMR was isolated by semipreparative HPLC (Merck Hibar C18 column, 10 × 250 mm). Elution was conducted at 4 mL/min with a gradient starting from 95% solvent A (0.1% trifluoroacetic acid in water) and 5% solvent B (0.1% trifluoroacetic acid in MeCN) to 5% solvent A and 95% solvent B for 30 minutes. The fractions containing PEG-peptide-^{18}F-TMR were pooled and dried with a rotary evaporator. PEG-peptide-^{18}F-TMR was dissolved in PBS and passed through a 0.22-μm filter (Millipore) into a sterile vial for use in animal experiments. The overall decay-corrected radiochemical yield of PEG-peptide-^{18}F-TMR was 15% (based on H^{18}F radioactivity). Quality control was conducted by analytic HPLC analysis (Merck Hibar C18 column, 4 × 250 mm; eluted at 1 mL/min with a gradient starting from 95% solvent A and 5% solvent B to 5% solvent A and 95% solvent B at 30 minutes). The radiochemical purity of PEG-peptide-^{18}F-TMR was greater than 95% by analytic HPLC analysis. The specific radioactivity of ^{18}F-SFB was estimated by radio-HPLC to be 4 TBq/mmol.

Specificity and serum half-life of PEG-peptide-^{18}F-TMR

A total of 1×10^5 HT1080 and MCF-7 cells were seeded overnight in DMEM containing 10% serum in 24-well plates at 37°C in a CO_2 incubator. The cells were cultured in serum-free DMEM for 48 hours before 3700 kBq PEG-peptide-^{18}F-TMR in the presence or absence of 10 μmol/L 1,10-phenanthroline (Sigma-Aldrich) at 37°C for 1 hours. The wells were washed to remove unbound probe, and the cells were collected by treatment with trypsin. The radioactivity of the cells was then measured in a γ-counter. BALB/c nude mice ($n = 3$) were intravenously injected with 3,700 kBq PEG-peptide-^{18}F-TMR, and blood samples were periodically removed from the tail vein of the mice. The blood was weighed on an analytical balance and assayed for radioactivity in a multichannel γ-counter. The initial and terminal half-life of the probe were estimated by fitting the data to a 2-phase exponential decay model with Prism 4 software (GraphPad Software).

Micro-PET Imaging of MMP activity *in vivo*

BALB/c nude mice ($n = 3$) bearing established HT1080 and MCF-7 tumors (100–200 mm^3) in their right and left hind leg, respectively, were anesthetized by halothane vapor with a vaporizer system and then were intravenously injected with 3,700 kBq (in 100 μL) PEG-peptide-^{18}F-TMR. PET imaging was sequentially conducted at 15, 60, and 120 minutes. To test the specificity of PEG-peptide-^{18}F-TMR *in vivo*, 1,10-phenanthroline (20 mg/kg/d for 3 days) or control vehicle was intraperitoneally injected into the mice ($n = 3$) 3 days prior to PEG-peptide-^{18}F-TMR injection. The tumor-bearing mice were positioned in a micro-PET scanner (R4; Concorde Microsystems) with their long axis parallel to the transaxial plane of the scanner. The scanner has a computer-controlled bed with a 10.8-cm transaxial and 8-cm axial field of view. It has no septa and operates exclusively in a 3-dimensional list mode. All raw data were first sorted into 3-dimensional sinograms, followed by Fourier rebinning and ordered subsets expectation maximization image reconstruction. Fully 3-dimensional list mode data were collected by using an energy window of 350 to 750 keV and a time window of 6 ns. Image pixel size was 0.85 mm transaxially, with a 1.21-mm section thickness. The region of interest (ROI) was analyzed with ASIPro VM version 5.0 (Concorde Microsystems) analysis software.

Statistical analysis

Statistical significance of differences between mean values was estimated with InStat software (version 3.0; GraphPad Software) using the independent Student *t* test for unequal variances. *P* values of less than 0.05 were considered statistically significant.

Results

Hydrolysis of peptide-TMR by MMP2 and MMP-expressing cells

To evaluate whether peptide-TMR could be selectively hydrolyzed by MMP, we incubated peptide-TMR (1,618 Da) with purified MMP2 or conditioned medium from MMP-expressing HT1080 cells or control MCF-7 cells. The cleaved fragments of peptide-TMR were detected by MALDI-TOF. We found that peptide-TMR (1,618 Da; Fig. 2A) could be cleaved by purified MMP2 to release TMR (948 Da; Fig. 2B). Treatment of peptide-TMR with culture medium from HT1080 cells produced similar results (Fig. 2C), whereas medium from MCF-7 cells was unable to cleave peptide-TMR (Fig. 2D). Cleavage of peptide-TMR was blocked by 1,10-phenanthroline, a broad-spectrum MMP inhibitor (refs. 23, 24; data not shown). These results show that peptide-TMR can be selectively hydrolyzed by MMP2 and MMP-expressing cells.

In vitro imaging of PEG-peptide-TMR in MMP-expressing cells

The conversion of peptide-TMR by MMP may be used to detect MMP activity if the hydrophobic TMR moiety preferentially localizes or accumulates at sites displaying MMP activity. Thus, we tested whether MMP-expressing HT1080 cells could activate and retain TMR-derived fluorescence. Figure 3A shows that strong fluorescence accumulated in HT1080 cells, but not control MCF-7 cells, indicating that TMR selectively accumulated at MMP-expressing HT1080 cells *in vitro*. Addition of MMP2 to MCF-7 cells resulted in fluorescence accumulation at the MCF-7 cells, indicating that the accumulation of TMR was dependent on MMP activity. On the other hand, addition of

Published OnlineFirst October 21, 2011; DOI:10.1158/1078-0432.CCR-11-0608

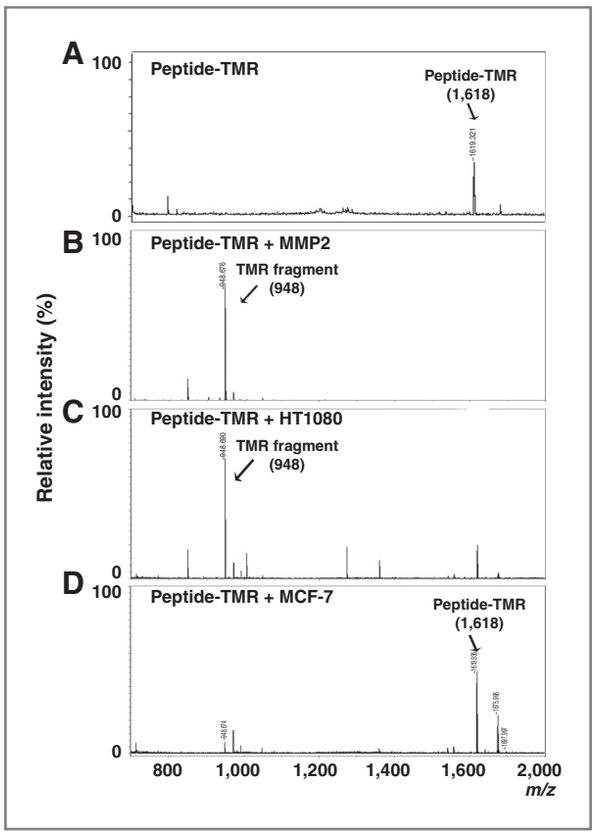

Figure 2. Characterization of MMP cleavage of peptide-TMR by MALDI-TOF. A, peptide-TMR (1,618 Da) was incubated with PBS (A) or with 1 unit of purified MMP2 (B) and the cleaved fragments were detected by MALDI-TOF. The major cleavage fragment of peptide-TMR (948 Da) is indicated by an arrow. Peptide-TMR incubated with culture medium from HT1080 cells (C) or MCF-7 cells (D) at 37°C for 1 hour. Cleavage of the peptide-TMR (948 Da) or intact peptide-TMR (1,618 Da) was detected by MALDI-TOF.

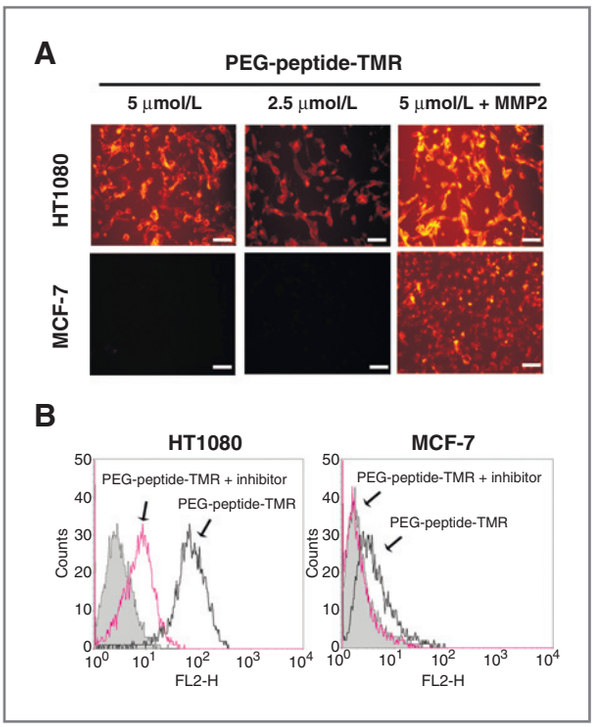

Figure 3. *In vitro* activation of PEG-peptide-TMR. A, HT1080 and MCF-7 cells were incubated with 2.5 or 5 μmol/L of PEG-peptide-TMR in the presence or absence of additional MMP2 at 37°C for 1 hour. TMR fluorescence was observed under a fluorescence microscope. B, HT1080 and MCF-7 cells were incubated with 5 μmol/L PEG-peptide-TMR in the presence (purple line) or absence (black line) of 10 μmol/L 1,10-phenanthroline at 37°C for 1 hour. Cell-bound fluorescence of viable cells was analyzed by flow cytometry. Scale bar, 100 μm.

1,10-phenanthroline to HT1080 cells significantly decreased the intensity of TMR fluorescence by more than 10-fold (Fig. 3B). Both TIMP-1 (a soluble MMP inhibitor) and TIMP-2 (a membrane-tethered and soluble MMP inhibitor) decreased TMR fluorescence intensity in HT1080 cells, showing that soluble MMPs were largely responsible for cleaving PEG-peptide-TMR (Supplementary Fig. S1).

Optical imaging of peptide-TMR activation and uptake of PEG-peptide-TMR at MMP-expressing tumors *in vivo*

To investigate whether PEG-peptide-TMR could noninvasively image MMP activity *in vivo*, mice bearing HT1080 and MCF-7 tumors were intravenously injected with PEG-peptide-TMR. Figure 4A shows that fluorescence signals accumulated in MMP-expressing HT1080 tumors but not in the control MCF-7 tumors, indicating that PEG-peptide-TMR was selectively converted to hydrophobic TMR fragments in HT1080 tumors. Serial imaging analysis revealed that the highest fluorescence was observed at 60 minutes after PEG-peptide-TMR injection, supporting earlier studies that probes can be activated and quickly accumulate in tumor areas (26). To verify the imaging results, the tumors were resected, and TMR fluorescence was immediately examined under a fluorescence microscope or stained with a commercial MMP2 substrate to confirm functional MMP expression *ex vivo*. Figure 4B shows red fluorescence concomitant with MMP expression (green fluorescence) in the HT1080 tumors but not control MCF-7 tumor sections, indicating the selective accumulation of TMR at the sites of MMP activity *in vivo*.

Specificity and half-life of PEG-peptide-^{18}F-TMR

We labeled PEG-peptide-TMR with ^{18}F to generate a PEG-peptide-^{18}F-TMR probe for PET imaging. We first evaluate whether PEG-peptide-^{18}F-TMR retained MMP2 selectivity *in vitro* by incubating HT1080 and MCF-7 cells with 37 kBq of PEG-peptide-^{18}F-TMR. Figure 5A shows that 36,900 ± 8,700 cpm accumulated at HT1080 cells, compared with 4,100 ± 550 cpm at control MCF-7 cells ($P < 0.01$). Furthermore, 1,10-phenanthroline decreased the accumulation of radioactivity to 940 ± 300 cpm at HT1080 cells ($P < 0.01$), suggesting that accumulation of the radioactivity indeed requires MMP activity. These results show that the PEG-peptide-^{18}F-TMR probe maintains high MMP

Published OnlineFirst October 21, 2011; DOI:10.1158/1078-0432.CCR-11-0608

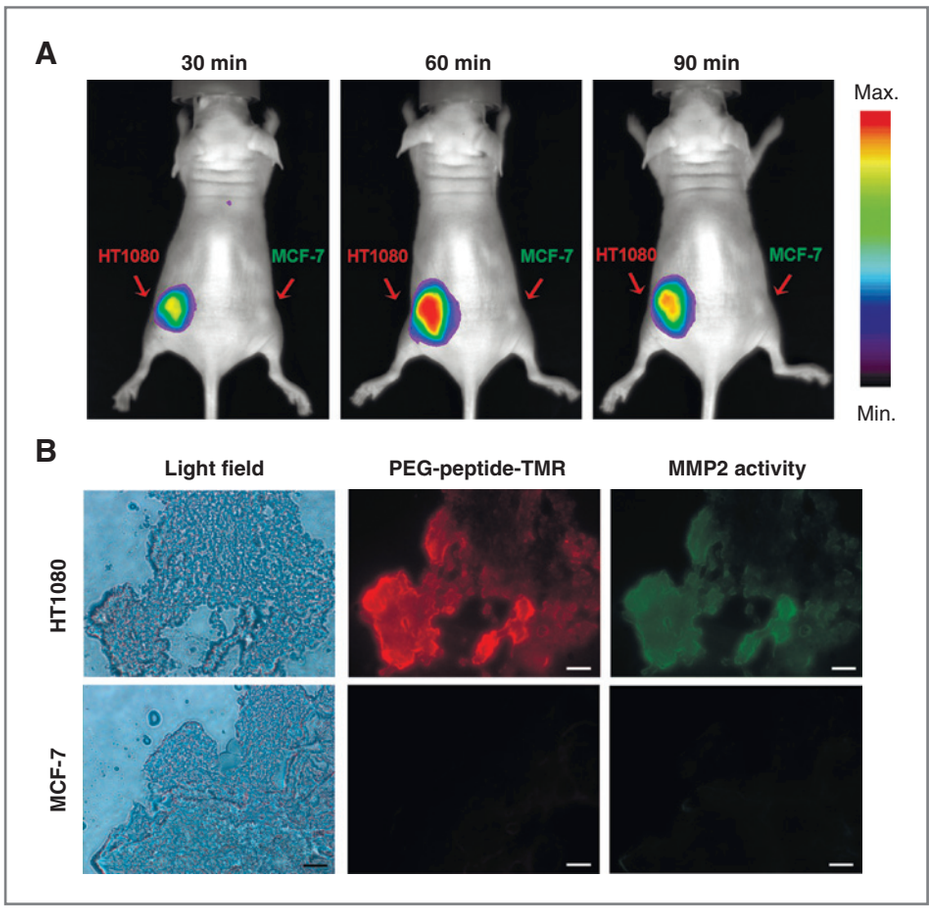

Figure 4. *In vivo* optical imaging of MMP activity. A, mice bearing established HT1080 (left hind legs) and MCF-7 (right hind legs) tumors were injected with 350 μmol/L PEG-peptide-TMR. Optical images were acquired at 30, 60, and 90 minutes after injection. B, mice bearing established HT1080 and MCF-7 tumors were injected with 350 μmol/L PEG-peptide-TMR and sacrificed 1 hour later. Sections of HT1080 (top) and MCF-7 (bottom) tumors were stained with 520 MMP-2 Assay Kit to detect MMP2 activity in tumor sections. TMR-derived fluorescence (red) and MMP2 activity (green) were observed under a fluorescence microscope. Scale bar, 1 mm.

selectivity *in vitro*. We also examined the half-life of PEG-peptide-^{18}F-TMR in the circulation of BALB/c mice at different time points following PEG-peptide-^{18}F-TMR injection. Figure 5B shows that the PEG-peptide-^{18}F-TMR was rapidly eliminated from the blood following 2-phase exponential decay kinetics with an initial half-life of 4.5 minutes and a terminal half-life of 36.5 minutes. Radioactivity in blood was as low as 0.2 ± 0.1 %ID/g at 2 hours after injection, indicating PEG-peptide-^{18}F-TMR was rapidly cleared from the circulation.

Micro-PET imaging of MMP activity *in vivo*

To evaluate whether PEG-peptide-^{18}F-TMR can detect MMP activity *in vivo*, mice bearing HT1080 and MCF-7 tumors were intravenously injected with PEG-peptide-^{18}F-TMR and imaged at different time points. Figure 6A shows that radiosignals selectively accumulated in HT1080 tumors but not in MCF-7 tumors. Serial imaging analysis indicated that the highest image intensity occurred at 60 minutes after injection of PEG-peptide-^{18}F-TMR, consistent with our optical imaging results. The radioactivity in the ROI was 3.7-, 17.4-, and 18.4-fold higher in HT1080 tumors than in MCF-7 tumors at 15, 60, and 120 minutes, respectively, suggesting that the PEG-peptide-^{18}F-TMR was preferentially hydrolyzed and accumulated in HT1080 tumors. Strong imaging intensity was observed in the kidneys of mice by PET, suggesting that the probe was eliminated via the urinary system (Supplementary Fig. S2). Moreover, radioactivity in the ROI was decreased by 1,10-phenanthroline treatment (Fig. 6B); following 1,10-phenanthroline treatment the radioactivity in the ROI was only 1.3-, 3.6-, and 3.3-fold greater in HT1080 tumors than in MCF-7 tumors at 15, 60, and 120 minutes. These results indicate that PEG-peptide-^{18}F-TMR can be used to detect tumoral MMP activity *in vivo* by micro-PET.

Biodistribution of PEG-peptide-^{18}F-TMR *in vivo*

HT1080 and MCF-7 tumor–bearing mice were intravenously injected with PEG-peptide-^{18}F-TMR, and the radioactivity in selected tissues was examined. Greater radioactivity was retained at HT1080 tumors than at control MCF-7 tumors at every time point examined (Supplementary Fig. S4). Highest tumoral uptake of ^{18}F-TMR (10.4 ± 1.3 %ID/g) was found at 60 minutes after injection. On average, HT1080 tumors accumulated 4.3 ± 0.8-, 18.4 ± 1.9-, and 20.4 ± 6.1-fold more radioactivity than in MCF-7 tumors at 15, 60, and 120 minutes, respectively. At earlier time points, the radioactivity retained in the kidneys was most likely attributable to the elimination of the radiolabeled probes in urine. These results show that PEG-peptide-^{18}F-TMR could

Published OnlineFirst October 21, 2011; DOI:10.1158/1078-0432.CCR-11-0608

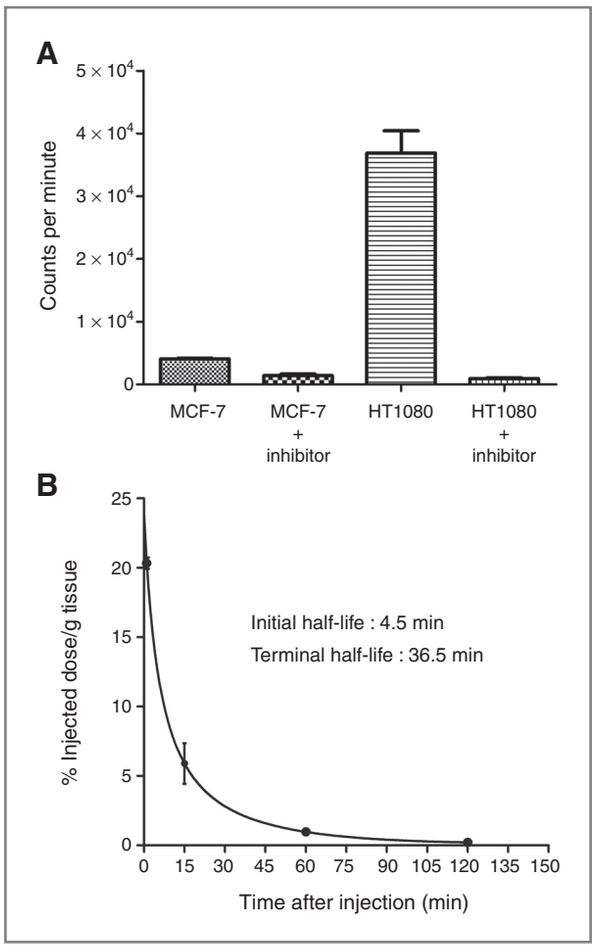

Figure 5. Specificity and serum half-life of PEG-peptide-^{18}F-TMR. A, HT1080 and MCF-7 cells were incubated with 37 kBq of PEG-peptide-^{18}F-TMR in the presence or absence of 10 μmol/L 1,10-phenanthroline at 37°C for 1 hour. Cellular radioactivity was measured in a γ-counter. B, kinetics of the PEG-peptide-^{18}F-TMR in serum. $t_{1/2} = 4.75$ minutes. Error bar, standard error of triplicate determinations.

be selectively activated and accumulated in MMP-expressing HT1080 tumors *in vivo*.

Discussion

We successfully developed a noninhibitory protease substrate probe for PET imaging of protease activity based on the conversion of PEG-peptide-^{18}F-TMR to ^{18}F-TMR *in vivo*. Our results show that PEG-peptide-TMR could be specifically converted into TMR fragments and accumulate at MMP-expressing HT1080 cells *in vitro* and *in vivo* by optical imaging. By PET imaging, PEG-peptide-^{18}F-TMR administration was found to allow preferential accumulation of ^{18}F-TMR in MMP-expressing HT1080 tumors as compared with control MCF-7 tumors. Thus, PEG-peptide-^{18}F-TMR, by means of MMP cleavage may aid in the development of personalized, protease-based prodrug-targeted therapies and for evaluating cancer prognosis based on the protease activity in patients.

Protease detection is important for diagnosis and to design personalized therapies for patients. Many methods have been developed to detect protease expression in the serum or tissues of patients, including real-time PCR (27, 28), immunohistochemistry (29), and ELISA (30). In additional, Ujula and colleagues reported the design of a ^{64}Ga-labeled MMP9-targeting peptide for imaging MMP9 expression *in vivo* by PET (31). However, proteases are generally expressed and secreted in inactive forms (2, 3). Methods that detect protease expression in serum or tissues may not reflect actual proteolytic activities. In our study, conversion of PEG-peptide-^{18}F-TMR to hydrophobic ^{18}F-TMR relies on proteolytic activities of MMPs. This probe represents a significant advancement in clinical imaging to measure actual protease activity in patients.

Modification of the peptide linker in PEG-peptide-^{18}F-TMR should allow development of probes to image different disease-associated proteases. Overexpression of proteases has been reported not only in cancers but also in many other diseases. For example, there are many enzyme-activated fluorescence probes that can be used to detect cysteine protease activity in atherosclerosis (32), virus protease activity in human immunodeficiency virus (HIV), hepatitis C virus (HCV) protease-expressing cells (33, 34), MMP activity in the myocardium after myocardial infarction (35), and cathepsin B activity in osteoarthritis and rheumatoid arthritis (36). The design of the PEG-peptide-^{18}F-TMR probe is based on the release of a hydrophobic moiety upon proteolytic cleavage. The peptide linker of PEG-peptide-^{18}F-TMR can be changed to allow imaging of other proteases. In addition, the TMR moiety can be easily linked to a wide variety of contrast agents, such as F^{18} for PET, ^{111}In-DOTA for SPECT, or Gd-DOTA for MRI, suggesting flexibility in choosing the optimal imaging system. We show here that MMP activity could be imaged by PET and optical imaging *in vivo*, implying that this strategy may be extended to other proteases in different diseases.

PET or SPECT imaging are considered to provide the highest sensitivity among the current imaging systems (37). However, optimal probes for PET/SPECT imaging of proteases have not yet been available. Up till now, protease inhibitors labeled with isotopes are used most frequently as SPECT- or PET-based imaging agents. For example, Sprague and colleagues reported the design of a ^{64}Cu-labeled MMP2/9-inhibitory peptide for imaging MMP expression *in vivo* by PET. Weak tumoral uptake of the probe and high tissue background were observed (38). In addition, many non-peptidyl MMP inhibitors have been used to image A549 tumors by radiolabeled valine-based biphenylsulphonamide MMP inhibitor tumors (39) or to image Kaposi sarcoma by ^{111}In-TIMPs (40), but the tumoral uptake of these imaging agent was low. Most of the existing MMP inhibitors have a broad range of affinities toward different MMP subtypes

Published OnlineFirst October 21, 2011; DOI:10.1158/1078-0432.CCR-11-0608

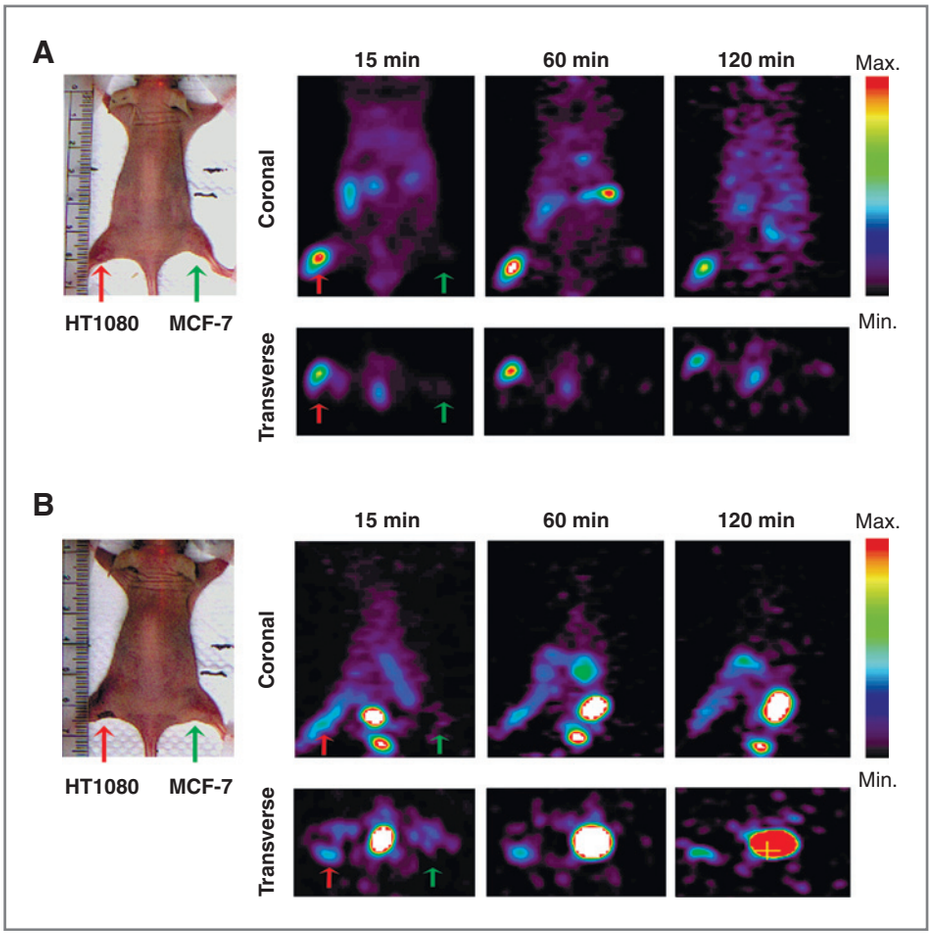

Figure 6. Micro-PET imaging of MMP activity *in vivo*. A, mice bearing established HT1080 (left hind legs) and MCF-7 (right hind legs) tumors were injected with 3,700 kBq of PEG-peptide-^{18}F-TMR. Coronal and transverse images of were acquired at 15, 60, and 120 minutes after injection. B, mice bearing established HT1080 (left hind legs) and MCF-7 (right hind legs) tumors were intraperitoneally injected with 1,10-phenanthroline (20 mg/kg/d for 3 days) before intravenous injection of PEG-peptide-^{18}F-TMR (3,700 kBq). Coronal and transverse images of tumor sections were acquired at 15, 60, and 120 minutes after injection of the probe.

(41, 42), limiting the specificity of this approach for protease-based prodrug-targeted therapy. Furthermore, the systemic delivery of protease inhibitors can induce undesirable side effects, such as musculoskeletal pain and inflammation, complications often not seen in preclinical models (43). When patients receive ongoing protease inhibitor therapy, imaging studies could be severely obscured if MMP inhibitor–based imaging probes are used in the same patients. Our noninhibitory protease substrate is cleaved and released by active proteases. An advantage in our noninhibitory design relates to the signal amplification by protease hydrolysis of copious probes which leads to increased imaging sensitivity and reduced dosage of imaging agents and thus probe-associated toxicities. Therefore, successful development of new noninhibitory protease probes may have better utility for clinical and experimental medicine.

Proteases are attractive enzymes for peptide- or inhibitor-based prodrug-targeted therapy (4, 6, 43–45). However, clinical trials targeting proteases have yielded disappointing results, mainly from administration of the drugs (46). It is important to better understand how protease activities change during tumor progression. In our strategy, noninhibitory protease substrates can accurately image protease activity at different stages, which may help clinicians choose the proper timing for protease prodrugs or inhibitor-based therapy to maximize treatment efficacy. This strategy may also aid in monitoring therapeutic responses to protease prodrugs/inhibitors.

Disclosure of Potential Conflicts of Interest

No potential conflicts of interest were disclosed.

Grant Support

This work was supported by grants from the National Research Program for Biopharmaceuticals (NSC 100-2325-B-037-001), Academia Sinica (AS-98-TP-B09), and the Department of Health, Executive Yuan, R.O.C. (DOH100-TD-N-111-010, DOH100-TD-C-111-002). The authors acknowledge technical support from the Molecular and Genetic Imaging Core (NSC98-3112-B-001) and are supported by the National Research Program for Genomic Medicine.

The costs of publication of this article were defrayed in part by the payment of page charges. This article must therefore be hereby marked *advertisement* in accordance with 18 U.S.C. Section 1734 solely to indicate this fact.

Received March 11, 2011; revised September 10, 2011; accepted September 20, 2011; published OnlineFirst October 21, 2011.

Published OnlineFirst October 21, 2011; DOI:10.1158/1078-0432.CCR-11-0608

References

1. Davies B, Waxman J, Wasan H, Abel P, Williams G, Krausz T, et al. Levels of matrix metalloproteases in bladder cancer correlate with tumor grade and invasion. Cancer Res 1993;53:5365–9.
2. Rao JS. Molecular mechanisms of glioma invasiveness: the role of proteases. Nat Rev Cancer 2003;3:489–501.
3. Stamenkovic I. Matrix metalloproteinases in tumor invasion and metastasis. Semin Cancer Biol 2000;10:415–33.
4. Folgueras AR, Pendas AM, Sanchez LM, Lopez-Otin C. Matrix metalloproteinases in cancer: from new functions to improved inhibition strategies. Int J Dev Biol 2004;48:411–24.
5. He Y, Liu XD, Chen ZY, Zhu J, Xiong Y, Li K, et al. Interaction between cancer cells and stromal fibroblasts is required for activation of the uPAR-uPA-MMP-2 cascade in pancreatic cancer metastasis. Clin Cancer Res 2007;13:3115–24.
6. Parsons SL, Watson SA, Steele RJ. Phase I/II trial of batimastat, a matrix metalloproteinase inhibitor, in patients with malignant ascites. Eur J Surg Oncol 1997;23:526–31.
7. Nelson AR, Fingleton B, Rothenberg ML, Matrisian LM. Matrix metalloproteinases: biologic activity and clinical implications. J Clin Oncol 2000;18:1135–49.
8. Chiappori AA, Eckhardt SG, Bukowski R, Sullivan DM, Ikeda M, Yano Y, et al. A phase I pharmacokinetic and pharmacodynamic study of s-3304, a novel matrix metalloproteinase inhibitor, in patients with advanced and refractory solid tumors. Clin Cancer Res 2007;13:2091–9.
9. Beattie GJ, Smyth JF. Phase I study of intraperitoneal metalloproteinase inhibitor BB94 in patients with malignant ascites. Clin Cancer Res 1998;4:1899–902.
10. Albright CF, Graciani N, Han W, Yue E, Stein R, Lai Z, et al. Matrix metalloproteinase-activated doxorubicin prodrugs inhibit HT1080 xenograft growth better than doxorubicin with less toxicity. Mol Cancer Ther 2005;4:751–60.
11. Stern L, Perry R, Ofek P, Many A, Shabat D, Satchi-Fainaro R. A novel antitumor prodrug platform designed to be cleaved by the endoprotease legumain. Bioconjug Chem 2009;20:500–10.
12. Roy R, Yang J, Moses MA. Matrix metalloproteinases as novel biomarkers and potential therapeutic targets in human cancer. J Clin Oncol 2009;27:5287–97.
13. Vihinen P, Kahari VM. Matrix metalloproteinases in cancer: prognostic markers and therapeutic targets. Int J Cancer 2002;99:157–66.
14. Kallakury BV, Karikehalli S, Haholu A, Sheehan CE, Azumi N, Ross JS. Increased expression of matrix metalloproteinases 2 and 9 and tissue inhibitors of metalloproteinases 1 and 2 correlate with poor prognostic variables in renal cell carcinoma. Clin Cancer Res 2001;7:3113–9.
15. Jiang T, Olson ES, Nguyen QT, Roy M, Jennings PA, Tsien RY. Tumor imaging by means of proteolytic activation of cell-penetrating peptides. Proc Natl Acad Sci U S A 2004;101:17867–72.
16. Law B, Curino A, Bugge TH, Weissleder R, Tung CH. Design, synthesis, and characterization of urokinase plasminogen-activator-sensitive near-infrared reporter. Chem Biol 2004;11:99–106.
17. Bremer C, Tung CH, Bogdanov A Jr, Weissleder R. Imaging of differential protease expression in breast cancers for detection of aggressive tumor phenotypes. Radiology 2002;222:814–8.
18. Jastrzebska B, Lebel R, Therriault H, McIntyre JO, Escher E, Guerin B, et al. New enzyme-activated solubility-switchable contrast agent for magnetic resonance imaging: from synthesis to *in vivo* imaging. J Med Chem 2009;52:1576–81.
19. Wagner S, Breyholz HJ, Law MP, Faust A, Holtke C, Schroer S, et al. Novel fluorinated derivatives of the broad-spectrum MMP inhibitors N-hydroxy-2(R)-[[(4-methoxyphenyl)sulfonyl](benzyl)- and (3-picolyl)-amino]-3-methyl-butanamide as potential tools for the molecular imaging of activated MMPs with PET. J Med Chem 2007;50:5752–64.
20. Zheng QH, Fei X, DeGrado TR, Wang JQ, Stone KL, Martinez TD, et al. Synthesis, biodistribution and micro-PET imaging of a potential cancer biomarker carbon-11 labeled MMP inhibitor (2R)-2-[[4-(6-fluorohex-1-ynyl)phenyl]sulfonylamino]-3-methylbutyric acid [11C]methyl ester. Nucl Med Biol 2003;30:753–60.
21. Watkins GA, Jones EF, Scott Shell M, VanBrocklin HF, Pan MH, Hanrahan SM, et al. Development of an optimized activatable MMP-14 targeted SPECT imaging probe. Bioorg Med Chem 2009;17:653–9.
22. Bae M, Cho S, Song J, Lee GY, Kim K, Yang J, et al. Metalloprotease-specific poly(ethylene glycol) methyl ether-peptide-doxorubicin conjugate for targeting anticancer drug delivery based on angiogenesis. Drugs Exp Clin Res 2003;29:15–23.
23. Fiore E, Fusco C, Romero P, Stamenkovic I. Matrix metalloproteinase 9 (MMP-9/gelatinase B) proteolytically cleaves ICAM-1 and participates in tumor cell resistance to natural killer cell-mediated cytotoxicity. Oncogene 2002;21:5213–23.
24. Moses MA, Wiederschain D, Loughlin KR, Zurakowski D, Lamb CC, Freeman MR. Increased incidence of matrix metalloproteinases in urine of cancer patients. Cancer Res 1998;58:1395–9.
25. Wust F, Hultsch C, Bergmann R, Johannsen B, Henle T. Radiolabelling of isopeptide N epsilon-(gamma-glutamyl)-L-lysine by conjugation with N-succinimidyl-4-[18F]fluorobenzoate. Appl Radiat Isot 2003;59:43–8.
26. Bremer C, Bredow S, Mahmood U, Weissleder R, Tung CH. Optical imaging of matrix metalloproteinase-2 activity in tumors: feasibility study in a mouse model. Radiology 2001;221:523–9.
27. Koga Y, Yasunaga M, Moriya Y, Akasu T, Fujita S, Yamamoto S, et al. Detection of colorectal cancer cells from feces using quantitative real-time RT-PCR for colorectal cancer diagnosis. Cancer Sci 2008;99:1977–83.
28. Walton TJ, Li G, McCulloch TA, Seth R, Powe DG, Bishop MC, et al. Quantitative RT-PCR analysis of estrogen receptor gene expression in laser microdissected prostate cancer tissue. Prostate 2009;69:810–9.
29. Zhang B, Cao X, Liu Y, Cao W, Zhang F, Zhang S, et al. Tumor-derived matrix metalloproteinase-13 (MMP-13) correlates with poor prognoses of invasive breast cancer. BMC Cancer 2008;8:83.
30. Ward AM, Catto JW, Hamdy FC. Prostate specific antigen: biology, biochemistry and available commercial assays. Ann Clin Biochem 2001;38:633–51.
31. Ujula T, Huttunen M, Luoto P, Perakyla H, Simpura I, Wilson I, et al. Matrix metalloproteinase 9 targeting peptides: syntheses, 68Ga-labeling, and preliminary evaluation in a rat melanoma xenograft model. Bioconjug Chem 2010;21:1612–21.
32. Jaffer FA, Vinegoni C, John MC, Aikawa E, Gold HK, Finn AV, et al. Real-time catheter molecular sensing of inflammation in proteolytically active atherosclerosis. Circulation 2008;118:1802–9.
33. Fuse T, Watanabe K, Kitazato K, Kobayashi N. Establishment of a new cell line inducibly expressing HIV-1 protease for performing safe and highly sensitive screening of HIV protease inhibitors. Microbes Infect 2006;8:1783–9.
34. Lei YF, Yin W, Yang J, Lv X, Wei SH, An QX, et al. Development of a cell-based assay for monitoring hepatitis C virus ns3/4a protease activity. Acta Virol 2008;52:133–41.
35. Chen J, Tung CH, Allport JR, Chen S, Weissleder R, Huang PL. Near-infrared fluorescent imaging of matrix metalloproteinase activity after myocardial infarction. Circulation 2005;111:1800–5.
36. Ji H, Ohmura K, Mahmood U, Lee DM, Hofhuis FM, Boackle SA, et al. Arthritis critically dependent on innate immune system players. Immunity 2002;16:157–68.
37. Madsen MT, Park CH. Enhancement of SPECT images by Fourier filtering the projection image set. J Nucl Med 1985;26:395–402.
38. Sprague JE, Li WP, Liang K, Achilefu S, Anderson CJ. *In vitro* and *in vivo* investigation of matrix metalloproteinase expression in metastatic tumor models. Nucl Med Biol 2006;33:227–37.
39. Oltenfreiter R, Staelens L, Kersemans V, Cornelissen B, Frankenne F, Foidart JM, et al. Valine-based biphenylsulphonamide matrix metalloproteinase inhibitors as tumor imaging agents. Appl Radiat Isot 2006;64:677–85.
40. Kulasegaram R, Giersing B, Page CJ, Blower PJ, Williamson RA, Peters BS, et al. *In vivo* evaluation of 111In-DTPA-N-TIMP-2 in Kaposi sarcoma associated with HIV infection. Eur J Nucl Med 2001;28:756–61.
41. Wagner S, Breyholz HJ, Faust A, Holtke C, Levkau B, Schober O, et al. Molecular imaging of matrix metalloproteinases *in vivo* using small

Published OnlineFirst October 21, 2011; DOI:10.1158/1078-0432.CCR-11-0608

molecule inhibitors for SPECT and PET. Curr Med Chem 2006;13: 2819–38.

42. Yang Y, Hong H, Zhang Y, Cai W. Molecular imaging of proteases in cancer. Cancer Growth Metastasis 2009;2:13–27.
43. Coussens LM, Fingleton B, Matrisian LM. Matrix metalloproteinase inhibitors and cancer: trials and tribulations. Science 2002;295:2387–92.
44. DiPaola RS, Rinehart J, Nemunaitis J, Ebbinghaus S, Rubin E, Capanna T, et al. Characterization of a novel prostate-specific antigen-activated peptide-doxorubicin conjugate in patients with prostate cancer. J Clin Oncol 2002;20:1874–9.
45. Mhaka A, Denmeade SR, Yao W, Isaacs JT, Khan SR. A 5-fluorodeoxyuridine prodrug as targeted therapy for prostate cancer. Bioorg Med Chem Lett 2002;12:2459–61.
46. Rothenberg ML, Carbone DP, Johnson DH. Improving the evaluation of new cancer treatments: challenges and opportunities. Nat Rev Cancer 2003;3:303–9.